CMS Physics Analysis Summary

Contact: cms-pag-conveners-susy@cern.ch 2016/03/07

Search for electroweak production of charginos in final states with two tau leptons in pp collisions at $\sqrt{s} = 8$ TeV

The CMS Collaboration

Abstract

A search for electroweak production of supersymmetric particles is performed with two tau leptons in the final state. These results are based on 18.1 to 19.6 fb^{-1} of proton-proton collisions at $\sqrt{s} = 8$ TeV, collected with the CMS detector at the CERN Large Hadron Collider. The observed events are found to be consistent with the standard model prediction. Upper limits are set on the masses of the lightest chargino and the lightest neutralino, assuming the third generation sleptons are the lightest sleptons and their masses are at a middle point between the chargino and the neutralino. In the context of simplified model spectra, charginos lighter than 417 GeV are excluded at 95% confidence level in the case of massless neutralino.

1 Introduction

Supersymmetry (SUSY) [1–5] is one of the most promising extensions of the standard model (SM) of elementary particles. It leads to the unification of gauge couplings at high energy, it mitigates the problem of quadratic divergences in quantum corrections to the mass of the Higgs boson, and, in its R-parity-conserving realization, provides a dark matter candidate. A key prediction of SUSY is the existence of new particles with the same properties as SM particles but differing in spin by half a unit ("sparticles").

Extensive searches at the CERN LHC have excluded the existence of colored sparticles with masses below a few hundred GeV to about 1 TeV, depending on the details of the assumed models [6–13]. On the other hand, the constraints on sparticles with only electroweak quantum numbers are much less stringent. This motivates the work described in this paper.

Searches for charginos, neutralinos, and sleptons by the CMS and ATLAS collaborations are described in Refs. [14–18]. In various SUSY models, the lightest SUSY partners of SM fermions are those from the third generation, resulting in enhanced branching fractions for final states with taus [19]. The previous searches for charginos, neutralinos, and sleptons by the CMS collaboration [14] are not performed for the case of the scalar τ lepton and its neutrino ($\tilde{\tau}$ and $\widetilde{\nu}_\tau$) to be the lightest sleptons. In this paper, a search for charginos is reported using events with two opposite-sign τ leptons and missing transverse momentum ($p_{\mathrm{T}}^{\mathrm{miss}}$), assuming the masses of the third-generation sleptons are between those of the chargino and the lightest neutralino. Two τ leptons can be generated in the decay chain of $\widetilde{\tau}$ or charginos ($\widetilde{\chi}_1^+$) as shown in Fig. 1. The

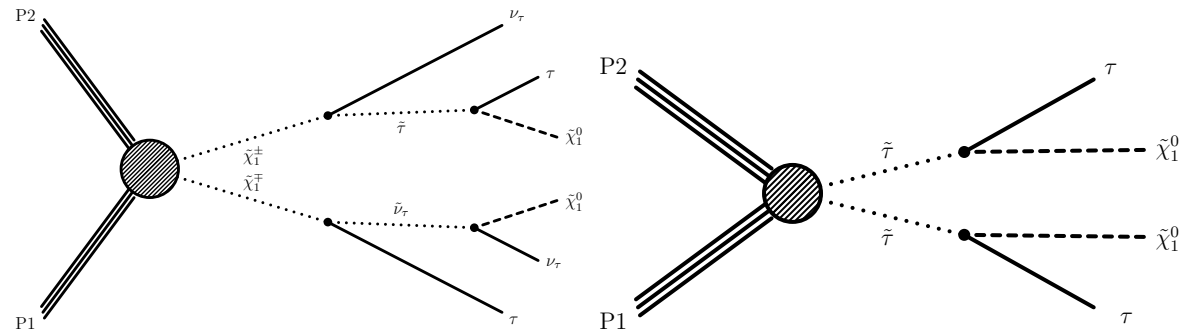

Figure 1: Schematic production of double τ from chargino pair and stau pair.

physics interpretation is provided in the context of Simplified Model Spectra (SMS) for SUSY [20, 21]. An ATLAS search for SUSY in di-tau final state is reported in Ref. [22], excluding chargino masses up to 345 GeV for a massless neutralino ($\widetilde{\chi}_1^0$).

The results discussed here are based on a dataset of proton-proton collisions at $\sqrt{s}$ = 8 TeV collected with the CMS detector at the CERN LHC during 2012, corresponding to integrated luminosities of 18.1 and 19.6 fb^{-1} in different channels. Our search makes use of the stransverse mass variable (M_{T2}) [23, 24] which is the natural extension of transverse mass (m_{T}) to the case where two massive particles with equal mass are created in pairs and decay to two invisible particles accompanied by jets and/or leptons. We consider final states where two taus are each reconstructed as a hadronic decay of a tau ($\tau_{\mathrm{h}}\tau_{\mathrm{h}}$), or where only one tau is reconstructed as the hadronic decay of a tau and the other one decays leptonically ($\ell\tau_{\mathrm{h}}$; ℓ = electron or muon).

The paper is organized as follows. The CMS detector, the event reconstruction, and the data sets are described in Sections 2 and 3; the M_{T2} variable is introduced in Section 4; the event selections for the two channels ($\tau_{\mathrm{h}}\tau_{\mathrm{h}}$ and $\ell\tau_{\mathrm{h}}$) are described in Sections 5 and 6, respectively; a detailed study of the SM backgrounds is presented in Section 7, while Section 8 is devoted

to the description of the systematic uncertainties. The result of the search with its statistical interpretation is presented in Section 9 and the paper is finally summarized in Section 10.

2 The CMS detector and event reconstruction

The central feature of the CMS apparatus is a superconducting solenoid of 6 m internal diameter, providing a magnetic field of 3.8 T. Within the superconducting solenoid volume are a silicon pixel and strip tracker, a lead tungstate crystal electromagnetic calorimeter (ECAL), and a brass and scintillator hadron calorimeter (HCAL), each composed of a barrel and two endcap sections. Muons are measured in gas-ionization detectors embedded in the steel flux-return yoke outside the solenoid. Extensive forward calorimetry complements the coverage provided by the barrel and endcap detectors. A more detailed description of the CMS detector, together with a definition of the coordinate system used and the relevant kinematic variables, can be found in Ref. [25].

Events from pp interactions must satisfy the requirements of a two-level trigger system. The first level (L1) of the CMS trigger system, composed of custom hardware processors, uses information from the calorimeters and muon detectors to select the most interesting events in a fixed time interval of less than 4 μs. The high-level trigger (HLT) processor farm further decreases the event rate from around 100 kHz to around 400 Hz, before data storage.

The particle-flow event algorithm [26, 27] reconstructs and identifies each individual particle with an optimized combination of information from the various elements of the CMS detector. Jets are reconstructed with the anti-k_T clustering algorithm [28] with a distance parameter of 0.5. We apply p_T- and η-dependent corrections to account for residual effects of non-uniform detector response [29]. A correction to account for multiple pp collisions within the same or a nearby bunch crossing (pileup interactions) is estimated on an event-by-event basis using the jet-area method described in Ref. [30], and is subtracted from the reconstructed jet p_T. The combined secondary vertex algorithm is used to identify ("b-tagged") jets originating from b-quarks. This algorithm is based on the reconstruction of secondary vertices, together with track-based lifetime information [31]. In this analysis the "medium" working point is used. The working point corresponds to an average b-tagged jets efficiency of 70%, light-quark jet misidentification rate of 1.5%, and c-quark jet misidentification rate of 20% for jets with a p_T value greater than 60 GeV. Jets with $p_T > 40$ GeV and $|\eta| < 5.0$ and b-tagged jets with $p_T > 20$ GeV and $|\eta| < 2.4$ are considered in this analysis.

The particles from the particle-flow algorithm are used to reconstruct the missing transverse momentum vector $\vec{p}_T^{\,miss}$, defined as the negative of the vector sum of the transverse momenta of all reconstructed particles. Corrections are applied to ensure consistency between $\vec{p}_T^{\,miss}$ and the corrections to jet energies described above. The missing transverse momentum in the event (p_T^{miss}) is defined as the magnitude of $\vec{p}_T^{\,miss}$.

Hadronically-decaying τ leptons, referred to as τ_h, are reconstructed using the hadron-plus-strips algorithm [32]. The constituents of the reconstructed jets are used to identify individual tau decay modes with one charged hadron and up to two neutral pions, or three charged hadrons. Additional discriminators are used to separate τ_h from electrons and muons. Prompt τ leptons are expected to be isolated in the detector. To discriminate them from QCD jets, we use a measure of isolation based on the charged hadrons and photons falling within a cone around the tau momentum direction after correcting for the effect of pileup. A similar isolation algorithm is used in this analysis to separate leptons (e or μ) from tau decays from those arising from hadron decays within jets.

3 Monte Carlo samples

Events from Z+jets, W+jets, $t\bar{t}$, and di-boson are generated using the MADGRAPH 5.1 [33] generator. Single-top-quark and Higgs boson events are generated by POWHEG 1.0 [34–37]. In the following figures and tables, the events containing at least one top quark and one Z boson are referred to as "Top" and "ZX", respectively. Events from Higgs boson production via gluon fusion, vector boson fusion or in association with a Z or W boson or a $t\bar{t}$ pair are referred to as "Higgs". The masses of the top quark and Higgs boson are set to be 172.5 GeV and 125 GeV, respectively.

In signal samples, a pair of $\widetilde{\chi}_1^{\pm}$ are produced and decay exclusively to the final states which contain two τ, two ν_τ and two neutralinos ($\widetilde{\chi}_1^0$) as shown in Fig. 1 (left). The mediators in the decay of $\widetilde{\chi}_1^{\pm}$ can be either a $\widetilde{\tau}$ or a $\widetilde{\nu}_\tau$. The masses of the $\widetilde{\tau}$ and the $\widetilde{\nu}_\tau$ are set to be equal and at the mean value of the $\widetilde{\chi}_1^{\pm}$ and $\widetilde{\chi}_1^0$ masses. Thus they are produced on-shell. The two distinct decay chains in the left diagram of Fig. 1 are assumed to have equal branching fractions of 50%. For parton shower and fragmentation, all generators are interfaced with PYTHIA 6.4 [38]. PYTHIA is also used to generate signal events (chargino pair production). To improve the modeling of τ decays, we use the TAUOLA 1.1.1a [39] package.

In the dataset considered in this paper, there were on average 21 proton-proton interactions ("pileup") in each bunch crossing. Additional interactions are generated with PYTHIA and superimposed on simulated events in a manner consistent with the luminosity profile of the dataset. The detector response in the Monte Carlo background event samples is modeled by a detailed simulation of the CMS detector based on GEANT4 [40]. On the other hand, in order to reduce computational requirements, signal events are processed by the CMS fast simulation [41] instead of GEANT4. All simulated events are reconstructed with the same algorithms as collision data.

The SM backgrounds are normalized using the most accurate calculations of the cross sections available in the literature. These cross sections correspond to the next-to-next-to-leading order (NNLO) accuracy for Z+jets [42] and W+jets [43] events. The cross section of $t\bar{t}$ simulated sample at full NNLO accuracy including the resummation of next-to-next-to-leading-logarithmic (NNLL) terms is used [44]. The event yields from di-boson production are normalized to the next-to-leading order (NLO) cross section taken from Ref. [45]. The RESUMMINO [46–48] calculations at NLO+NLL are used to calculate the signal cross sections, where NLL refers to next-to-leading-logarithmic precision.

4 Definition of M_{T2}

The M_{T2} variable [23, 24] is used in this analysis to discriminate between the SUSY signal and the SM backgrounds as proposed in Ref. [49]. The variable was introduced to measure the mass of primary pair-produced particles, decaying eventually to undetected particles (e.g. $\widetilde{\chi}_1^0$). Assuming the two primary supersymmetric particles undergo the same decay chain with visible and undetectable particles in the final state, the system can be described by the visible mass ($m^{\mathrm{vis}(i)}$), transverse energy ($E_{\mathrm{T}}^{\mathrm{vis}(i)}$), and transverse momentum ($\vec{p}_{\mathrm{T}}^{\,\mathrm{vis}(i)}$) of each branch ($i = 1, 2$), together with the missing transverse momentum ($\vec{p}_{\mathrm{T}}^{\,\mathrm{miss}}$) which is shared between the two decay chains. The $\vec{p}_{\mathrm{T}}^{\,\mathrm{miss}}$ is interpreted as the sum of the transverse momenta of the neutralinos, $\vec{p}_{\mathrm{T}}^{\,\widetilde{\chi}_1^0(i)}$. However, in practice, in decay chains with neutrinos, $\vec{p}_{\mathrm{T}}^{\,\mathrm{miss}}$ includes contributions from the p_{T} of the neutrinos.

The transverse mass of each branch can be written as

$$(m_T{}^{(i)})^2 = (m^{\mathrm{vis}(i)})^2 + m^2_{\tilde{\chi}^0_1} + 2(E_T^{\mathrm{vis}(i)} E_T^{\tilde{\chi}^0_1(i)} - \vec{p}_T^{\,\mathrm{vis}(i)} \cdot \vec{p}_T^{\,\tilde{\chi}^0_1(i)}). \quad (1)$$

Using the correct neutralino mass, this distribution has an endpoint at the mass of the primary particle [50–53]. For a given $m_{\tilde{\chi}^0_1}$, the M_{T2} variable is defined as

$$M_{T2}(m_{\tilde{\chi}^0_1}) = \min_{\vec{p}_T^{\,\tilde{\chi}^0_1(1)} + \vec{p}_T^{\,\tilde{\chi}^0_1(2)} = \vec{p}_T^{\,\mathrm{miss}}} \left[\max \{ m_T{}^{(1)}, m_T{}^{(2)} \} \right]. \quad (2)$$

For the correct value of $m_{\tilde{\chi}^0_1}$, the kinematic endpoint of the M_{T2} distribution is at the mass of the primary particle, and it shifts accordingly when the assumed $m_{\tilde{\chi}^0_1}$ is lower or higher than the correct value. In this analysis, the visible part of the decay chain consists of either the two hadronically decaying tau leptons ($\tau_h\tau_h$ channel) or a combination of a muon or an electron with a τ_h candidate ($\ell\tau_h$ channel), so $m^{\mathrm{vis}(i)}$ is the mass of a lepton and can be set to zero. We also set $m_{\tilde{\chi}^0_1} = 0$.

With our choices of $m_{\tilde{\chi}^0_1}$ and $m^{\mathrm{vis}(i)}$, the resulting M_{T2} value is close to zero for the back-to-back topology of $\tau_h\tau_h$ or $\ell\tau_h$ events (e.g., Drell-Yan events; QCD di-jets if two jets are misidentified as τ_h objects), regardless of the values of p_T^{miss} and the p_T of the tau candidates. This is not the case for signal events where the taus or leptons are generally not in a back-to-back topology due to the presence of two undetected neutralinos.

The distribution of M_{T2} reflects the scale of the produced particles and is much higher for heavy sparticles compared to the lighter SM particles. Hence, SUSY could manifest itself as an excess of events in the high-side tail of the M_{T2} distribution.

5 Event selection for the $\tau_h\tau_h$ channel

In this channel events are first selected with a trigger [54–56] that requires the existence of two loosely identified, isolated τ_h candidates with $p_T > 35\,\mathrm{GeV}$ and $|\eta| < 2.1$.

Offline, the two τ_h candidates must pass the medium working point [32] of τ isolation discriminator, fulfill $p_T > 45\,\mathrm{GeV}$ and $|\eta| < 2.1$, and be of opposite charge. In events with more than one $\tau_h\tau_h$ pair, we only consider the pair with the most isolated τ_h objects.

Events with isolated extra electrons or muons of $p_T > 10\,\mathrm{GeV}$ and $|\eta| < 2.4$ are rejected to suppress backgrounds from diboson decays. The background from $Z \to \tau_h\tau_h$ events is reduced by rejecting events where the visible di-τ_h invariant mass is between 55 and 85 GeV (Z veto). Furthermore, contributions from low-mass Drell-Yan and QCD multijet production are reduced by requiring the invariant mass to be greater than 15 GeV. To reject $Z \to \tau_h\tau_h$ and QCD multijet events, $p_T^{\mathrm{miss}} > 30\,\mathrm{GeV}$ and $M_{T2} > 40\,\mathrm{GeV}$ are required. The minimum angle $\Delta\phi$ in the transverse plane between the $\vec{p}_T^{\,\mathrm{miss}}$ and any of the τ_h and jets, including b-tagged jets, must be greater than 1. This requirement reduces backgrounds from QCD multijet events and W+jets events.

After applying the pre-selection described above, additional requirements are introduced to define two search regions. The first search region (SR1) targets the models with large mass difference (Δm) between charginos and neutralinos. In this case, the M_{T2} signal distribution can have long tail beyond the distribution of SM backgrounds. The second search region (SR2)

is dedicated to models with small Δm. In this case, the sum of the two transverse mass values, $\Sigma m_{\mathrm{T}}^{\tau_i} = m_{\mathrm{T}}(\tau_{\mathrm{h}}^1, p_{\mathrm{T}}^{\mathrm{miss}}) + m_{\mathrm{T}}(\tau_{\mathrm{h}}^2, p_{\mathrm{T}}^{\mathrm{miss}})$, provides additional discrimination between signal and SM background processes.

The two signal regions (SR) are defined as:

- **SR1**: $M_{\mathrm{T2}} > 90\,\mathrm{GeV}$;
- **SR2**: b-tagged jets are vetoed; $M_{\mathrm{T2}} < 90\,\mathrm{GeV}$; and $\Sigma m_{\mathrm{T}}^{\tau_i} > 250\,\mathrm{GeV}$.

The veto on b-tagged jets in SR2 is to reduce $t\bar{t}$ events, which are expected in the low M_{T2} region. The SM backgrounds are validated with data-driven methods whenever possible and described in Section 7.

6 Event selection for the $\ell\tau_{\mathrm{h}}$ channel

Events in the $\ell\tau_{\mathrm{h}}$ final states ($\mathrm{e}\tau_{\mathrm{h}}$ and $\mu\tau_{\mathrm{h}}$) were collected with triggers that require a loosely isolated τ_{h} with $p_{\mathrm{T}} > 20\,\mathrm{GeV}$ and $|\eta| < 2.3$ as well as an isolated electron or muon with $|\eta| < 2.1$. The minimum p_{T} requirement for the electron (muon) was increased during the data taking from 20 to 22 GeV (17 to 18 GeV) due to the increase in instantaneous luminosity.

In the offline analysis, the electron, muon, and τ_{h} objects are required to have $p_{\mathrm{T}} > 25$, 20, and 25 GeV, respectively, while tightening the corresponding identification and isolation requirements. In events with more than one opposite-sign $\ell\tau_{\mathrm{h}}$ pair, we only consider the pair that maximizes the scalar sum of τ_{h} and electron or muon transverse momenta. Events with an additional loosely isolated lepton with $p_{\mathrm{T}} > 10\,\mathrm{GeV}$ are rejected to suppress backgrounds from Z boson decays.

Just like for the $\tau_{\mathrm{h}}\tau_{\mathrm{h}}$ channel, we apply preselection requirements to suppress QCD multijet, $\mathrm{t\bar{t}}$, $Z \to \tau\tau$, and low mass resonance events. These requirements are: $M_{\mathrm{T2}} > 40\,\mathrm{GeV}$, $p_{\mathrm{T}}^{\mathrm{miss}} > 30\,\mathrm{GeV}$, $\ell\tau_{\mathrm{h}}$ invariant mass between 15 and 45 GeV or $> 75\,\mathrm{GeV}$, $\Delta\phi > 1$. We reject events with b-tagged jets. The final signal region requirements are $M_{\mathrm{T2}} > 90\,\mathrm{GeV}$ and $m_{\mathrm{T}}^{\tau_{\mathrm{h}}} > 200\,\mathrm{GeV}$. The latter requirement provides discrimination against the W+jets background. Unlike the $\tau_{\mathrm{h}}\tau_{\mathrm{h}}$ channel, events with $M_{\mathrm{T2}} < 90\,\mathrm{GeV}$ are not used because of the higher level of background. Table 1 summarizes the selection requirements for different signal regions.

Table 1: Definition of different signal regions. OS stands for opposite-sign pairs.

$\ell\tau_{\mathrm{h}}$	$\tau_{\mathrm{h}}\tau_{\mathrm{h}}$ SR1	$\tau_{\mathrm{h}}\tau_{\mathrm{h}}$ SR2
OS $\ell\tau_{\mathrm{h}}$	OS $\tau_{\mathrm{h}}\tau_{\mathrm{h}}$	
$p_{\mathrm{T}}^{\mathrm{miss}} > 30\,\mathrm{GeV}$		
Extra lepton veto		
Invariant mass of $\ell\tau_{\mathrm{h}}$ or $\tau_{\mathrm{h}}\tau_{\mathrm{h}} > 15\,\mathrm{GeV}$		
Z boson mass veto		
$\Delta\phi > 1$		
$M_{\mathrm{T2}} > 40\,\mathrm{GeV}$		
b-tagged jet veto	-	b-tagged jet veto
$M_{\mathrm{T2}} > 90\,\mathrm{GeV}$		$M_{\mathrm{T2}} < 90\,\mathrm{GeV}$
$m_{\mathrm{T}}^{\tau_{\mathrm{h}}} > 200\,\mathrm{GeV}$	-	$\Sigma m_{\mathrm{T}}^{\tau_i} > 250\,\mathrm{GeV}$

Figure 2 shows the M_{T2} distribution after the preselection. The data are in good agreement

with the SM expectations within the statistical uncertainties. A SUSY signal corresponding to a high mass difference ($m_{\tilde{\chi}_1^\pm} = 380\,\text{GeV}$, $m_{\tilde{\chi}_1^0} = 1\,\text{GeV}$) is used to show the expected signal distribution.

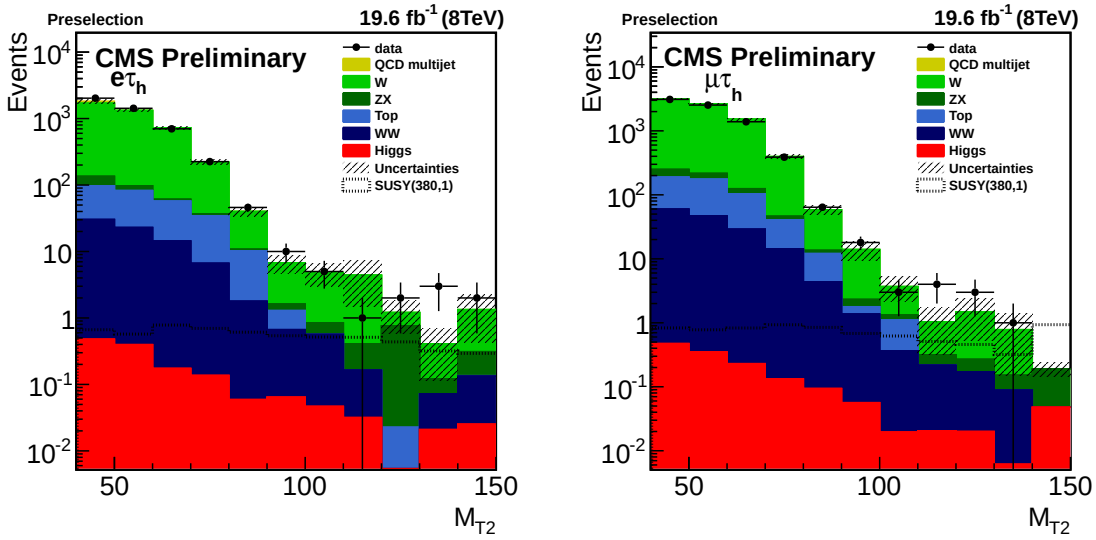

Figure 2: M_{T2} distributions for events in the sample after preselection, compared to SM expectation in (left) $e\tau_\text{h}$ and (right) $\mu\tau_\text{h}$ channels. The signal distribution is shown for $m_{\tilde{\chi}_1^\pm} = 380\,\text{GeV}$, $m_{\tilde{\chi}_1^0} = 1\,\text{GeV}$.

7 Backgrounds

The backgrounds are studied in two categories, those with "misidentified" τ_h, i.e., events where a quark or gluon jet has been misidentified as a τ_h, and those with real τ_h decays. QCD and W+jets events are dominant sources in the first category, while $\text{t}\bar{\text{t}}$, Z+jets, Higgs boson and diboson events in the second category. Background estimates are performed with data-driven methods whenever possible. Otherwise data-to-simulation scale factors are used to correct or to validate the expected contributions obtained from the simulated samples. The estimates of the main backgrounds are discussed below.

7.1 QCD background estimation in the $\tau_\text{h}\tau_\text{h}$ channel

Events from QCD multijet production can appear in the signal regions if two quark or gluon jets are misidentified as a $\tau_\text{h}\tau_\text{h}$ pair. The isolation variable is a powerful discriminant between misidentified and real τ_h objects. To estimate QCD multijet contribution, a set of $\tau_\text{h}\tau_\text{h}$ control regions (CR) is defined by relaxing the τ_h isolation requirement (from "medium" to "loose") and relaxing the M_{T2} or $\Sigma m_\text{T}^{\tau_i}$ requirements (from $M_{\text{T2}} > 90\,\text{GeV}$ to $M_{\text{T2}} > 40\,\text{GeV}$ and from $\Sigma m_\text{T}^{\tau_i} > 250\,\text{GeV}$ to $\Sigma m_\text{T}^{\tau_i} > 100\,\text{GeV}$). To reduce contamination from real $\tau_\text{h}\tau_\text{h}$ events in the control regions with at least one loose τ_h object, same-sign (SS) $\tau_\text{h}\tau_\text{h}$ pairs are selected. Residual contributions from real $\tau_\text{h}\tau_\text{h}$ and W+jets events (non-QCD events) are subtracted based on Monte Carlo expectations. The control regions and signal region are illustrated in Fig. 3. In the sample dominated by QCD multijet events (CR1 and CR2), the isolation of misidentified τ_h objects is verified to be almost completely uncorrelated with M_{T2} or $\Sigma m_\text{T}^{\tau_i}$. In addition, the requirement on $\Delta\phi$ is removed to increase the numbers of events in the control regions. The QCD background in the signal region is estimated by counting events in the control regions

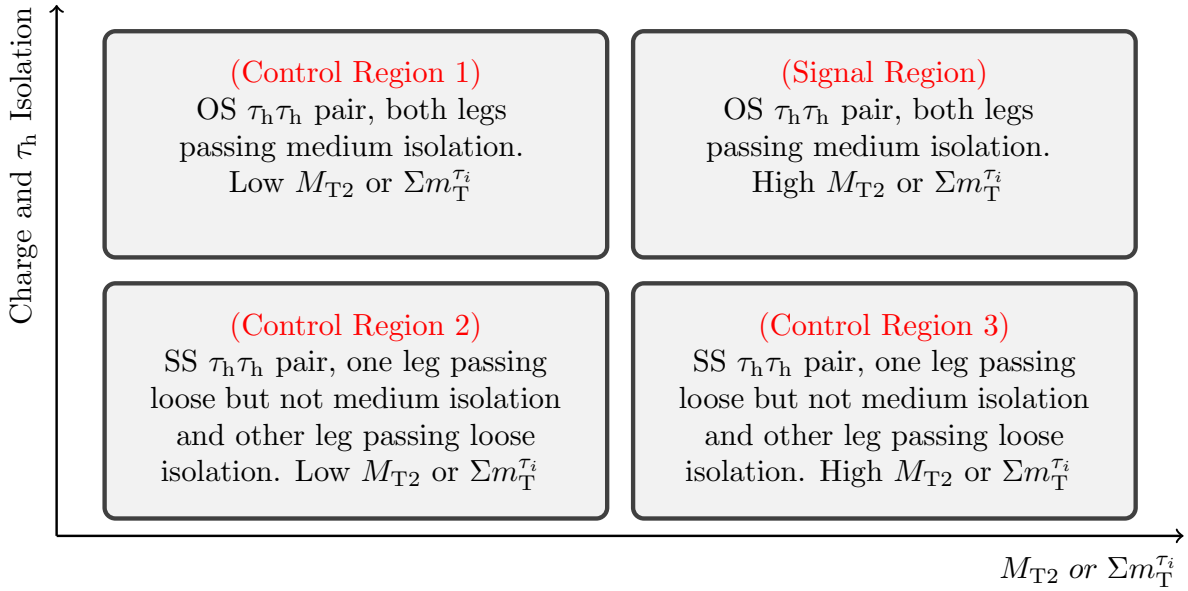

Figure 3: Schematic illustration of four control regions used to estimate the QCD backgrounds. SS and OS stand for same-sign and opposite-sign pairs.

with high M_{T2} or $\Sigma m_T^{\tau_i}$ and loosely isolated SS $\tau_h\tau_h$ (CR3) and scaling by the transfer factor to go from loosely isolated SS to tightly isolated opposite-sign (OS) $\tau_h\tau_h$ which is evaluated in the low M_{T2} or $\Sigma m_T^{\tau_i}$ regions (CR1 divided by CR2). The final estimate of the background is corrected by the efficiency of the $\Delta\phi$ requirement for QCD events. The latter efficiency is measured in CR1 and CR2, which are dominated by QCD multijet events. The efficiency is a falling distribution as the function of the search variable (M_{T2} or $\Sigma m_T^{\tau_i}$) and the value of the closest bin to CR3 ($65 < M_{T2} < 90\,\text{GeV}$ or $200 < \Sigma m_T^{\tau_i} < 250\,\text{GeV}$) is used conservatively as the value of the efficiency in CR3.

The systematic uncertainties are associated with the uncertainty on the validity of the assumption that isolation and M_{T2} or $\Sigma m_T^{\tau_i}$ are not correlated and the systematic uncertainties on the residual SM backgrounds which are subtracted based on Monte Carlo expectations. The latter includes both the statistical uncertainty of the simulated events and also a 22% systematic uncertainty that will be discussed in Section 8 assigned uniformly to all simulated events.

The number of data events in CR3 after subtracting the non-QCD events is 4.81 ± 2.57 (8.62 ± 3.55) in SR1 (SR2). The transfer factors are measured to be 0.91 ± 0.12 and 0.89 ± 0.11 in the low M_{T2} and $\Sigma m_T^{\tau_i}$, respectively, and the correction for the $\Delta\phi$ efficiency is 0.03 ± 0.04 in SR1 and 0.15 ± 0.08 in SR2. All reported uncertainties are the quadratic sum of the statistical and systematic uncertainties.

Table 2 summarizes the estimation of the QCD background contribution in the two signal re-

Table 2: The estimated QCD multijet background event yields in the $\tau_h\tau_h$ channel. The first two uncertainties are statistical and systematic uncertainties of the method, the last uncertainty is the extra systematic uncertainty due to correlation assumptions.

Signal Region	QCD Estimation
$\tau_h\tau_h$ SR1	$0.13 \pm 0.06(\text{stat}) \pm 0.18(\text{sys}) \pm 0.10(\text{fit})$
$\tau_h\tau_h$ SR2	$1.15 \pm 0.39(\text{stat}) \pm 0.70(\text{sys}) \pm 0.25(\text{fit})$

gions after extrapolation from the control regions and correcting for the $\Delta\phi$ efficiency. The uncertainties due to the statistic of the CR3 is reported as the statistical uncertainty "stat" and the other uncertainties are shown as "sys". To evaluate the uncertainties for transfer factor and $\Delta\phi$ efficiency due to correlation assumptions, different fit models are tested. Fitting the whole range of the low values of the search variables by a horizontal line or a line with a constant slope or using the value of the last bin before entering the signal region are examined. The weighted average of the estimates is compared with the reported values in Table 2 to extract the uncertainty shown as "fit" in the table.

7.2 W+jets background estimation in the $\tau_h\tau_h$ channel

The contribution of the W+jets background in $\tau_h\tau_h$ channels is taken from simulated events. The simulation is validated using a data control sample:

$$N_{SR} = N_{\text{Before Final Selection}} \times \epsilon_{FS}. \quad (3)$$

Here N_{SR} is the estimation of W+jets events in the signal region. $N_{\text{Before Final Selection}}$ is the number of W+jets events before applying the final selection ($M_{T2} > 90\,\text{GeV}$ for SR1 and $\Sigma m_T^{\tau_i} > 250\,\text{GeV}$ for SR2), but after applying all other selections, including $M_{T2} > 40\,\text{GeV}$ for SR1 and $40 < M_{T2} < 90\,\text{GeV}$ for SR2. ϵ_{FS} is $\epsilon_{M_{T2}} = \frac{N(M_{T2}>90)}{N(M_{T2}>40)}$ for SR1 or $\epsilon_{\Sigma m_T^{\tau_i}} = \frac{N(\Sigma m_T^{\tau_i}>250)}{N(40<M_{T2}<90)}$ for SR2. $N_{\text{Before Final Selection}}$ is 31.93±6.40 and 29.13±6.22 for SR1 and SR2, respectively, where the given uncertainties arise from the limited number of simulated events.

The efficiency of the final selection (ϵ_{FS}) is first evaluated in a W+jets simulated sample with a pair of opposite-sign τ_h where the τ_h candidates are selected with the same identification requirements as the signal region, but with looser kinematic selection to improve statistics. Additional signal selection requirements, such as $\Delta\phi$ or lepton veto, are applied one by one such that two orthogonal subsamples (passing and failing) are obtained. The ϵ_{FS} quantity is calculated in all subsamples. The values are found to be consistent within the statistical uncertainties; their weighted average is taken as the final estimate for ϵ_{FS} with weights corresponding to the size of the simulated sample at each step. The measured ϵ_{FS} are 0.029 ± 0.007 and 0.058 ± 0.015 for SR1 and SR2, respectively. The uncertainty of the τ_h energy scale is also taken into account in the uncertainty on ϵ_{FS}.

The W+jets simulated sample is validated in data using a same-sign $\mu\tau_h$ control sample, where both the normalization and ϵ_{FS} are checked. The ratio of data and Monte Carlo expectation is found to be 1.05 ± 0.13 (1.02 ± 0.09) for SR1 (SR2) which is compatible with unity, within the uncertainties. For ϵ_{FS}, to take into account the difference between the data and Monte Carlo values, the Monte Carlo prediction in each of the two signal regions is corrected by the ratio of the two values which is 0.73 ± 0.57 (1.49 ± 0.38) for SR1 (SR2) and its uncertainty is also taken to be the systematic uncertainty and referred to as "shape".

Table 3 summarizes the results of the method for different signal regions of the $\tau_h\tau_h$ channel.

7.3 Drell-Yan background estimation

The Drell-Yan (DY) background yield is obtained from Monte Carlo simulation. The simulated sample includes decay to different lepton pairs (ee, $\mu\mu$ and $\tau\tau$). The contribution from $Z \to \ell\ell$ and $Z \to \tau\tau \to \ell\ell$ events is found to be very small, because the misidentification probability for $\ell \to \tau_h$ is significantly low. The dominant events are $Z \to \tau\tau \to \ell\tau_h$ and $Z \to \tau\tau \to \tau_h\tau_h$ decays. The misidentification probability for $\tau_h \to \ell$ is also low, so the probability to have contribution from $Z \to \tau\tau \to \tau_h\tau_h$ events in the $\ell\tau_h$ channels is negligible. The simulation is

Table 3: The W+jets estimation results in both search regions. The systematic uncertainty "sys" comes from the maximum variation of the estimation found from varying the τ_h energy scale within its uncertainty. The "shape" takes into account the difference between the shape of the search variable distribution in data and simulation.

Signal Region	W+jets Estimation
$\tau_h\tau_h$ SR1	0.72 ± 0.11 (stat) $\pm$ 0.11 (sys) $\pm$ 0.56 (shape)
$\tau_h\tau_h$ SR2	2.58 ± 0.35 (stat) $\pm$ 1.04 (sys) $\pm$ 0.69 (shape)

validated in a $\mu\tau_h$ control region obtained by removing the $\Delta\phi$ requirement and by inverting the Z boson veto and also by requiring $M_{T2} < 20\,\text{GeV}$, $40 < m_T^{\tau_h} < 100\,\text{GeV}$. The distributions of invariant mass of $\mu\tau_h$ system for data and simulated events are in a good agreement. The transverse momentum of the Z boson system, which is correlated with M_{T2}, is also well reproduced in simulation. Table 4 summarizes the DY contribution in different signal regions. For

Table 4: DY background yield expected in four signal regions. Only the statistical uncertainties are reported.

Signal Region	DY Estimation
$e\tau_h$	0.19 ± 0.04
$\mu\tau_h$	0.25 ± 0.06
$\tau_h\tau_h$ SR1	0.56 ± 0.07
$\tau_h\tau_h$ SR2	0.81 ± 0.56

$\ell\tau_h$ channels, only the contributions from the real lepton + τ_h are reported. A separate method is developed to estimate the misidentified contamination in these channels in the Section 7.4.

7.4 Misidentified τ_h in the $\ell\tau_h$ channels

This contribution is estimated using a method that takes into account the probability that a loosely isolated misidentified or real τ_h, passes the tight isolation. If the signal selection is done using the τ_h objects which pass the "loose" isolation instead of "tight", the number of loose τ_h objects (N_{Loose}) is:

$$N_{\text{Loose}} = N_{\text{Real}} + N_{\text{Fake}} \tag{4}$$

where N_{Real} is the number of real τ_h objects and N_{Fake} is the number of misidentified τ_h objects. If the selection is tightened, the number of tight τ_h objects (N_{Tight}) is

$$N_{\text{Tight}} = r_{\text{Real}} \times N_{\text{Real}} + r_{\text{Fake}} \times N_{\text{Fake}} \tag{5}$$

where r_{Real} (r_{Fake}) is the real (fake) rate, the probability that a loosely selected real (misidentified) τ_h object passes the tight selection. One can obtain the following expression by eliminating N_{Real}:

$$N_{\text{Fake}} \times (r_{\text{Fake}} - r_{\text{Real}}) = (N_{\text{Tight}} - r_{\text{Real}} \times N_{\text{Loose}}) \tag{6}$$

Here $r_{\text{Fake}} \times N_{\text{Fake}}$ is the contamination of misidentified τ_h objects to the signal region.

The fake rate (r_{Fake}) is measured as the ratio of tightly selected τ_h objects to loosely selected τ_h objects in a sample which is dominated by misidentified τ_h objects. This is done in a data sample with same selection as $\ell\tau_h$, except a reversed p_T^{miss} requirement, i.e., $p_T^{\text{miss}} < 30\,\text{GeV}$. The fake rate is measured to be 0.54 ± 0.01. The real rate (r_{Real}) is measured in simulated DY events, and it is found to be $r_{\text{Real}} = 0.766 \pm 0.003$ and almost independent of M_{T2}. A conservative relative systematic uncertainty of 5% is assigned to the central value of r_{Real} to cover its fluctuations in different values of M_{T2}. To validate the method, it is applied to a W+jets simulated sample when the fake rate is evaluated in this simulated sample with the same method as used for data. The result is close to $r_{\text{Fake}} = 0.54$. To cover the difference, a 5% relative systematic uncertainty is assigned to the central values of the fake rates. The method correctly predicts the number of $\ell\tau_h$ background events in this sample, within the uncertainties. These include statistical uncertainties due to the number of events in the sidebands (loosely selected τ_h) as well as systematic uncertainties. The uncertainties on the fake rate and the real rate are negligible compared to the statistical uncertainties associated with the sidebands.

The estimates of the misidentified τ_h contamination in the two $\ell\tau_h$ channels are summarized in Table 5. The relative statistic and systematic uncertainties are reported separately. Since

Table 5: Estimation of the misidentified τ_h contribution in the signal region of the $\ell\tau_h$ channels. The total systematic is the quadrature sum of the fractional systematics. All uncertainties are relative. r_{Fake} (r_{Real}) is shorthand for fake (real) rate.

Channel	Total Fake	stat	r_{Fake} sys	r_{Real} sys	Total Unc
$\mu\tau_h$	8.15	56%	18%	5%	59%
$e\tau_h$	3.30	101%	17%	2%	102%

the fake rate and real rate are in common between the two $\ell\tau_h$ channels, the total systematic uncertainties are considered fully correlated between the two channels.

8 Systematic uncertainties

Systematic uncertainties can affect the shape or normalization of the backgrounds estimated from simulation ($t\bar{t}$, Z+jets, dibosons and Higgs boson), as well as the signal acceptance. The uncertainties are listed below and summarized in Table 6.

- The energy scales for electron, muon and τ_h objects affect the shape of various kinematical distributions. The systematic uncertainties in the muon and electron energy scales are negligible. The visible energy of τ_h object in the Monte Carlo simulation is scaled up and down by 3%, and all τ_h-related variables are recalculated. The resulting variations in final yields are taken as the systematic uncertainties. They amount to 10-15% for backgrounds and 2-15% in different parts of the signal phase space.
- The uncertainty in electron and muon trigger, identification, and isolation efficiencies is 2% [57].
- The uncertainty in the τ_h identification efficiency is 6%. The uncertainty in the trigger efficiency of the τ_h leg of the $e\tau_h$ and $\mu\tau_h$ ($\tau_h\tau_h$) triggers amount to 3.0% (4.5% per leg). A "tag-and-probe" technique on $Z \to \tau\tau$ events is used to estimate the uncertainties [57].
- The uncertainty due to the scale factor on the b-tagging efficiency and mis-tag rate is evaluated by varying the factors within their uncertainties. The yields of signal and

Table 6: Summary of systematic uncertainties that affect the signal event selection efficiency and the background normalization and their shape. The sources that alter the shape are indicated by (*) next to their names. The shape-altering sources are considered correlated between two signal regions of $\tau_h\tau_h$ in the final statistical combination.

	Background			Signal		
Systematic uncertainty source	$\ell\tau_h$	$\tau_h\tau_h$ SR1	$\tau_h\tau_h$ SR2	$\ell\tau_h$	$\tau_h\tau_h$ SR1	$\tau_h\tau_h$ SR2
τ_h energy scale (*)	10%	15%		2-12%	3-15%	
τ_h id efficiency	6%	12%		6%	12%	
τ_h trigger efficiency	3%	9%		3%	9%	
Lepton trigger, id, iso efficiency	2%	-		2%	-	
p_T^{miss} (*)	5%			5%		
b-tagged jets veto	4%	-	4%	8%	-	8%
Pile-up	4%			4%		
Fast/Full τ_h id efficiency	-			5%	10%	
ISR (*)	-			3%		
$\Delta\phi_{min}$	-			6%		
PDF (*)	-			2%		
Luminosity	-			2.6%		
Total shape-altering sys.	11%	16%	16%	6-13%	7-16%	
Total non-shape-altering sys.	9%	16%	16%	14%	20%	21%
Total Systematic	14%	22%	22%	15-19%	21-25%	22-26%
Monte Carlo Statistic	22%	13%	70%	3-15%		
Total	26%	26%	73%	15-24%	21-29%	22-30%
Low rate backgrounds	50%			-		

background events are changed by 8% and 4%, respectively [31].

- To evaluate the uncertainty due to pileup, the measured inelastic pp cross-section is varied by 5% [58], resulting in a change in the number of simulated pileup interactions. The relevant acceptances for signal and background events are changed by 4%.
- The uncertainty in the signal acceptance due to parton distribution function uncertainties is taken to be 2% from a similar analysis [14].
- The uncertainty on the luminosity is 2.6% [59]. This affects mainly the normalization of the signal Monte Carlo samples, because for the backgrounds either the data-driven methods are used or the normalization is found from data.
- The uncertainty in the signal acceptance associated with initial state radiation (ISR) is evaluated by comparing the efficiencies of jet-related requirements between PYTHIA and MADGRAPH which is a matrix-element event generator. Using the SM WW process which is expected to be similar to chargino pair-production in terms of parton content and process, we assign a 3% uncertainty in the efficiency of b-tagged jets veto and a 6% uncertainty in the $\Delta\phi$ requirement. The ISR uncertainty is not considered for the background samples, due to the usage of matrix- element event generators.
- The uncertainties related to p_T^{miss} can arise from different sources e.g. the energy scales of lepton, τ_h, and jet objects and unclustered energy. The "unclustered energy" is the energy of the reconstructed objects which do not belong to any jet or lepton with $p_T > 10$ GeV. The effect of lepton and τ_h energy scales is discussed above. The contribution from the uncertainty of the jet energy scale (2-10% depending on η and

p_T) and unclustered energy (10%) is found to be negligible. A conservative value of 5% uncertainty is assigned to both signal and background processes based on Monte Carlo simulation studies [14, 16].

- The statistic of the simulated Monte Carlo samples is also a source of the uncertainty. This uncertainty amounts to 3-15% for the different parts of the signal phase space and 13-70% for the backgrounds in different signal regions.
- The performance of the fast detector simulation has some differences compared to the full detector simulation, especially in track reconstruction [16]. It can affect the τ_h isolation. A 5% systematic uncertainty per τ_h leg is assigned by comparing the τ_h isolation/identification efficiency in the fast and full simulations.
- For less important backgrounds like $t\bar{t}$, dibosons and Higgs boson, the remaining number of events from the simulation are very small. A 50% uncertainty is considered for these backgrounds to account for the possible theoretical uncertainty of the cross section calculation as well as the shape mismodeling.

The systematic uncertainties that can alter the shapes are added in quadrature and treated as correlated when two signal regions of $\tau_h\tau_h$ channel are combined. Other systematic uncertainties of these two channels and all of the systematic uncertainties of $\ell\tau_h$ channels are treated as uncorrelated.

9 Results and interpretation

The observed data and predicted background yields for the four signal regions are summarized in Table 7. In all signal regions the observed data are consistent with the predicted SM values

Table 7: Data yields and background predictions with uncertainties in the four signal regions of the search. The uncertainties are reported in two parts, which are statistics and systematic uncertainty, respectively. The main backgrounds (W+jets and QCD multijet) are derived from data as described in Section 7. "VV" is a shorthand for diboson events.

	$e\tau_h$	$\mu\tau_h$	$\tau_h\tau_h$ SR1	$\tau_h\tau_h$ SR2
Z+jets	$0.19 \pm 0.04 \pm 0.03$	$0.25 \pm 0.06 \pm 0.04$	$0.56 \pm 0.07 \pm 0.12$	$0.81 \pm 0.56 \pm 0.18$
$t\bar{t}$, VV, Higgs	$0.03 \pm 0.03 \pm 0.02$	$0.19 \pm 0.09 \pm 0.09$	$0.19 \pm 0.03 \pm 0.09$	$0.75 \pm 0.35 \pm 0.38$
W+jets	$3.30 \pm 3.35 \pm 0.56$	$8.15 \pm 4.59 \pm 1.53$	$0.72 \pm 0.11 \pm 0.57$	$2.58 \pm 0.35 \pm 1.25$
QCD multijet	-	-	$0.13 \pm 0.06 \pm 0.21$	$1.15 \pm 0.39 \pm 0.74$
SM Total	$3.52 \pm 3.35 \pm 0.56$	$8.59 \pm 4.59 \pm 1.53$	$1.60 \pm 0.15 \pm 0.62$	$5.29 \pm 0.70 \pm 1.51$
Observed	3	5	1	2

within the uncertainties.

Figure 4 compares the data and the SM expectation in four search regions. The top row shows the M_{T2} distributions in the $\ell\tau_h$ channels. In these plots, the QCD multijet and W+jets and fake contribution from other channels are based on the estimate described in Section 7.4 and labeled "W". The QCD multijet contribution is very low for these channels and is counted among "W". The bottom row shows the M_{T2} and $\Sigma m_T^{\tau_i}$ distributions in two different signal regions of $\tau_h\tau_h$ channel. The QCD multijet contribution in these plots is obtained using the data driven method described in Section 7.1. The W+jets contribution in the last bin of the bottom plots is described in Section 7.2, while the other bins are based on simulated events. The uncertainty band in these four plots, includes both the statistical and systematic uncertainties.

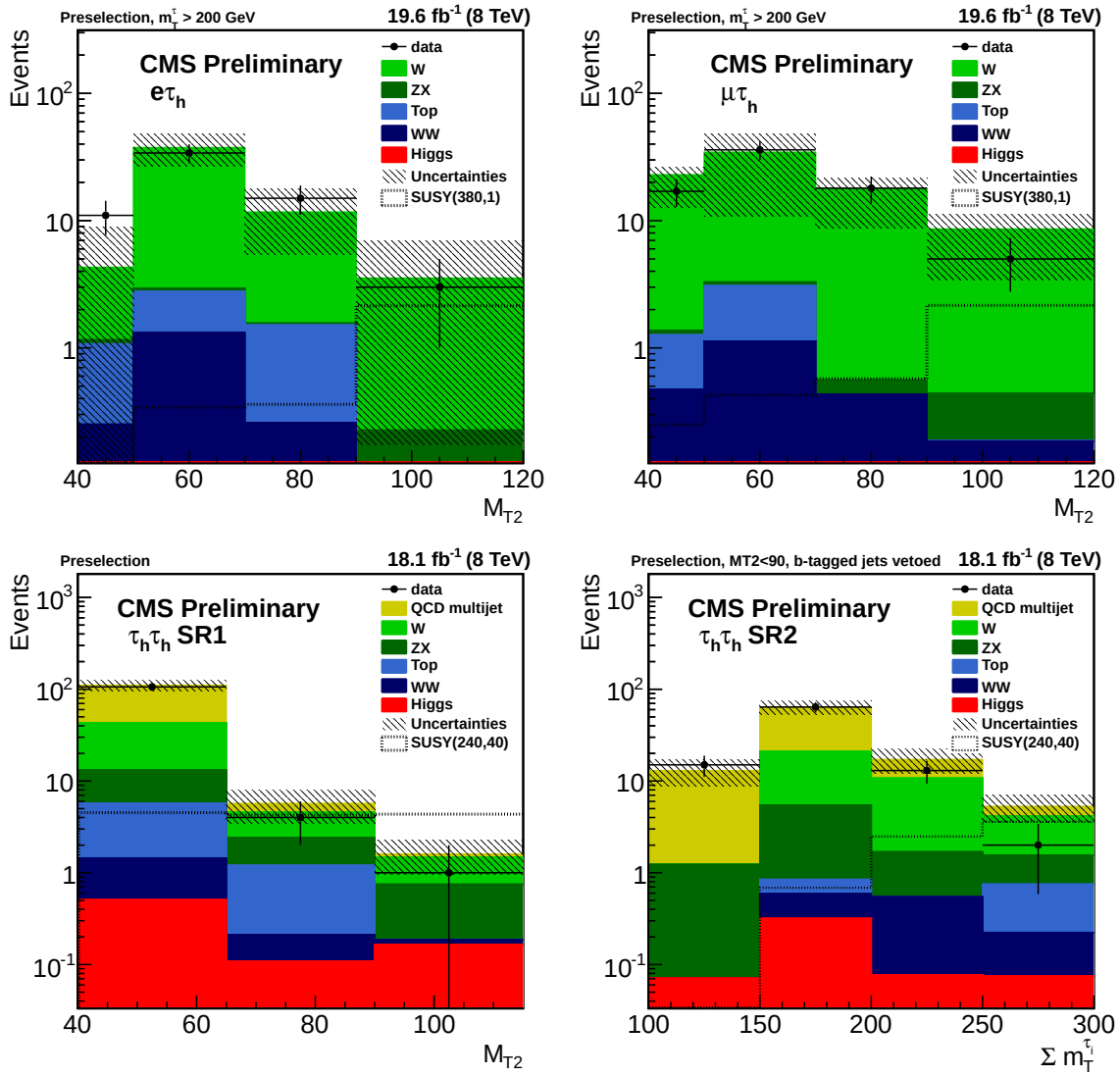

Figure 4: The data yield is compared with the SM expectation. In different signal regions, when a data driven background is available, it is used instead of the pure simulation. For more details read the text.

There is no excess of events over the SM expectation. We interpret our results in the context of a simplified model of chargino pair production and decay, which is described in Section 3 and corresponds to the left diagram in Fig. 1.

A modified frequentist approach, known as the CLs method [60], is used to set limits on cross sections at 95% confidence level. Combining all four signal regions, the observed limits rule out $\widetilde{\chi}_1^{\pm}$ masses up to 417 GeV for a massless $\widetilde{\chi}_1^0$. The results on excluded regions are shown in Fig. 5. This should be compared to the ATLAS limit of 345 GeV [22]. It should be noted that the ATLAS results are based on $\tau_h\tau_h$ channel. Figure 6 shows our results in the $\tau_h\tau_h$ channel, where the $\widetilde{\chi}_1^{\pm}$ masses are excluded up to 395 GeV for a massless $\widetilde{\chi}_1^0$. A stringent limit is obtained with our selection requirements where the SM background events are optimally reduced.

The $\widetilde{\tau}$ searches in the LEP experiments [61] have excluded masses below 95 GeV. In Fig. 5 and 6, this region corresponds to the triangle in bottom-left corner. The diagonal line denotes the boundary for $m_{\widetilde{\chi}_1^{\pm}} = m_{\tau} + m_{\widetilde{\chi}_1^0}$, which is the kinematical boundary of the search. The ex-

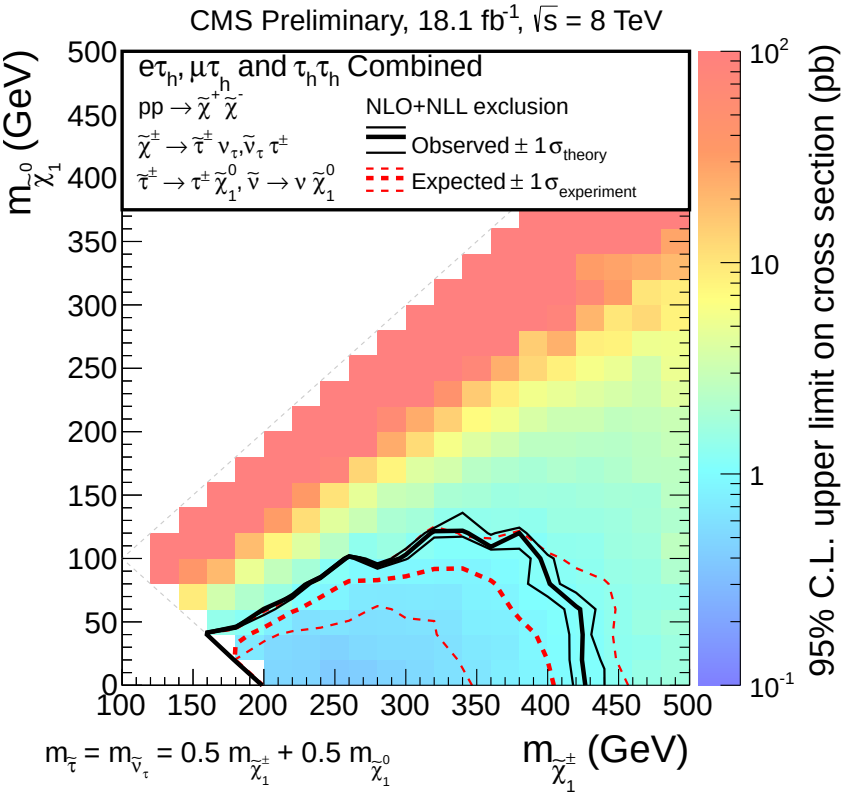

Figure 5: Expected and observed exclusion regions in terms of Simplified Models of chargino pair production with the total dataset of 2012. The bottom-left triangle was excluded by LEP $\tilde{\tau}$ searches. The diagonal line denotes the boundary for $m_{\tilde{\chi}_1^\pm} = m_\tau + m_{\tilde{\chi}_1^0}$. The $\pm$ 1 standard deviations of the expected (observed) exclusions introduced by the experimental (theoretical) uncertainties are also shown.

pected limits and their $\pm$ 1 standard deviations introduced by the experimental uncertainties are shown with the red solid and dashed lines, respectively. The observed limits are shown with a black solid line, while the $\pm$ 1 standard deviations based on signal cross section uncertainties are shown with narrower black lines. The signal cross sections in NLO + NLL order in α_s are used to make the exclusion limits. In the whole region, the observed limits are within one standard deviation from the expected limits.

The results of the $\tau_h\tau_h$ channels are also interpreted to set limit on the $\tilde{\tau}\,\tilde{\tau}$ production, which corresponds to the right diagram in Fig. 1. In this simplified model, two $\tilde{\tau}$ are directly produced from the pp collision and decay instantly into two τ and two $\tilde{\chi}_1^0$. Two $\ell\tau_h$ channels are not considered in this interpretation, because they do not improve the results. To calculate the production cross section, $\tilde{\tau}$ is defined as a maximal admixture of the left-handed and right-handed $\tilde{\tau}$ gauge-eigenstates [48]. As the cross section of direct production of sleptons is lower, no point is excluded and a 95% upper limit is set on the cross section as a function of the $\tilde{\tau}$ mass. Figure 7 represents the ratio of the obtained upper limit on the cross section and the cross section expected from SUSY (signal strength) vs. the mass of the $\tilde{\tau}$ particle, when $\tilde{\chi}_1^0$ mass is 1 GeV. The observed ratio is within one standard deviation of the expected ratio. The best limit, which corresponds to the lowest signal strength, is obtained for $m_{\tilde{\tau}} = 150$ GeV. The observed (expected) upper limit on the cross section at this mass is 43 (56) fb which is almost two times larger than the theoretical NLO cross section.

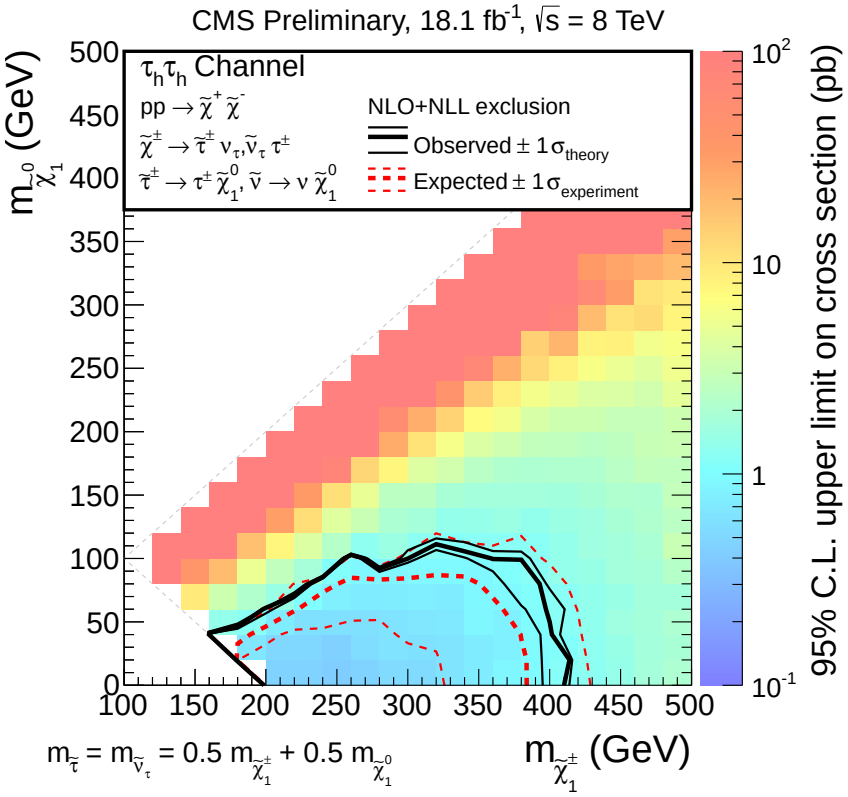

Figure 6: Expected and observed exclusion regions in terms of Simplified Models in $\tau_h\tau_h$ channel. The conventions are same as Fig. 5.

10 Conclusion

A search for SUSY in the $\tau\tau$ final state was performed where the τ pair could be produced in a cascade decay from the electroweak production of $\widetilde{\chi}_1^{\pm}$ pair in proton-proton collisions at $\sqrt{s}$ = 8 TeV, collected by the CMS detector. To maximize the sensitivity, event selections are optimized for $\tau_h\tau_h$ (small Δ M), $\tau_h\tau_h$ (large Δ M) and $\ell\tau_h$ channels using M_{T2}, $m_T^{\tau_h}$ and $\Sigma m_T^{\tau_i}$ variables. Events are consistent with the SM expectations. In the context of simplified models, charginos lighter than 417 GeV for a massless neutralino are excluded at 95% confidence level. The upper limits for the direct stau pair production are also provided, but the limits are more than three times larger than the theoretical NLO cross sections even for a massless neutralino.

References

[1] Y. A. Golfand and E. P. Likhtman, "Extension of the algebra of Poincare group generators and violation of p invariance", *JETP Lett.* **13** (1971) 452.

[2] J. Wess and B. Zumino, "A lagrangian model invariant under supergauge transformations", *Phys. Lett. B* **49** (1974) 52, doi:10.1016/0370-2693(74)90578-4.

[3] J. Wess and B. Zumino, "Supergauge transformations in four-dimensions", *Nucl. Phys. B* **70** (1974) 39, doi:10.1016/0550-3213(74)90355-1.

[4] P. Fayet, "Spontaneously broken supersymmetric theories of weak, electromagnetic and strong interactions", *Phys. Lett. B* **69** (1977) 489, doi:10.1016/0370-2693(77)90852-8.

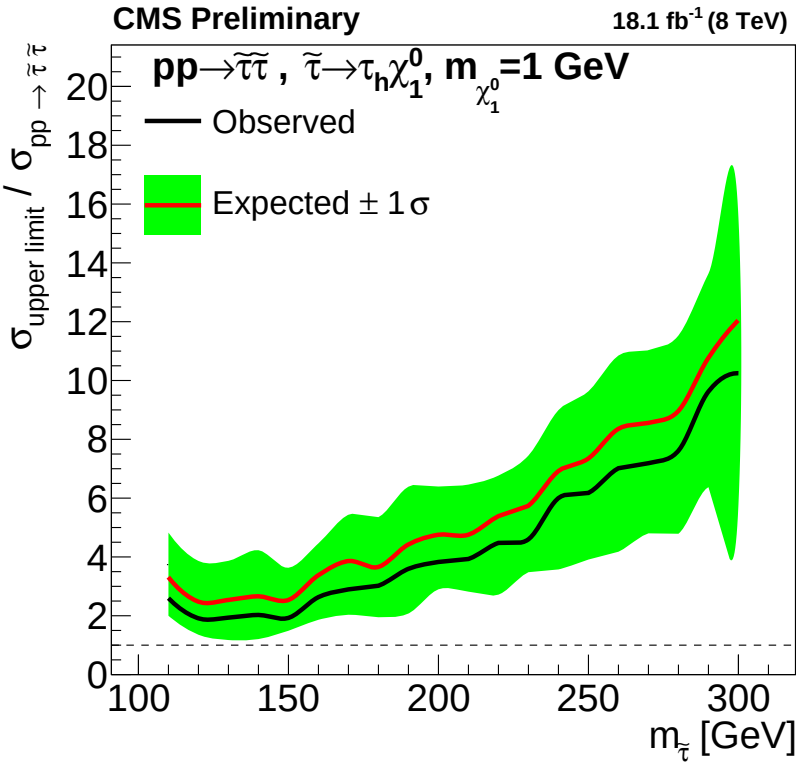

Figure 7: Upper limits on $\tilde{\tau}\,\tilde{\tau}$ production cross section in $\tau_h\tau_h$ channel. The mass of $\tilde{\chi}_1^0$ is 1 GeV.

[5] G. R. Farrar and P. Fayet, "Phenomenology of the production, decay, and detection of new hadronic states associated with supersymmetry", *Phys. Lett. B* **76** (1978) 575, doi:10.1016/0370-2693(78)90858-4.

[6] CMS Collaboration, "Search for new physics in events with same-sign dileptons and jets in pp collisions at $\sqrt{s}$ = 8 TeV", *JHEP* **01** (2014) 163, doi:10.1007/JHEP01(2015)014, 10.1007/JHEP01(2014)163, arXiv:1311.6736. [Erratum: JHEP01,014(2015)].

[7] CMS Collaboration, "Search for supersymmetry in hadronic final states with missing transverse energy using the variables α_T and b-quark multiplicity in pp collisions at $\sqrt{s} = 8$ TeV", *Eur. Phys. J.* **C73** (2013) 2568, doi:10.1140/epjc/s10052-013-2568-6, arXiv:1303.2985.

[8] CMS Collaboration, "Search for anomalous production of events with three or more leptons in pp collisions at $\sqrt{(s)} = 8$ TeV", *Phys. Rev.* **D90** (2014) 032006, doi:10.1103/PhysRevD.90.032006, arXiv:1404.5801.

[9] CMS Collaboration, "Search for new physics in the multijet and missing transverse momentum final state in proton-proton collisions at $\sqrt{s}$= 8 TeV", *JHEP* **06** (2014) 055, doi:10.1007/JHEP06(2014)055, arXiv:1402.4770.

[10] CMS Collaboration, "Searches for Supersymmetry using the M_{T2} Variable in Hadronic Events Produced in pp Collisions at 8 TeV", *JHEP* **05** (2015) 078, doi:10.1007/JHEP05(2015)078, arXiv:1502.04358.

[11] CMS Collaboration, "Search for Physics Beyond the Standard Model in Events with Two Leptons, Jets, and Missing Transverse Momentum in pp Collisions at sqrt(s) = 8 TeV", *JHEP* **04** (2015) 124, doi:10.1007/JHEP04(2015)124, arXiv:1502.06031.

[12] ATLAS Collaboration, "ATLAS Run 1 searches for direct pair production of third-generation squarks at the Large Hadron Collider", *Eur. Phys. J.* **C75** (2015), no. 10, 510, doi:10.1140/epjc/s10052-015-3726-9, arXiv:1506.08616.

[13] ATLAS Collaboration, "Summary of the searches for squarks and gluinos using $\sqrt{s} = 8$ TeV pp collisions with the ATLAS experiment at the LHC", *JHEP* **10** (2015) 054, doi:10.1007/JHEP10(2015)054, arXiv:1507.05525.

[14] CMS Collaboration, "Searches for electroweak production of charginos, neutralinos, and sleptons decaying to leptons and W, Z, and Higgs bosons in pp collisions at 8 TeV", *Eur.Phys.J.* **C74** (2014) 3036, doi:10.1140/epjc/s10052-014-3036-7, arXiv:1405.7570.

[15] CMS Collaboration, "Searches for electroweak neutralino and chargino production in channels with Higgs, Z, and W bosons in pp collisions at 8 TeV", *Phys. Rev.* **D90** (2014) 092007, doi:10.1103/PhysRevD.90.092007, arXiv:1409.3168.

[16] CMS Collaboration, "Search for supersymmetry in the vector-boson fusion topology in proton-proton collisions at $\sqrt{s} = 8$ TeV", *JHEP* **11** (2015) 189, doi:10.1007/JHEP11(2015)189, arXiv:1508.07628.

[17] ATLAS Collaboration, "Search for direct production of charginos and neutralinos in events with three leptons and missing transverse momentum in $\sqrt{s} = 8$TeV pp collisions with the ATLAS detector", *JHEP* **04** (2014) 169, doi:10.1007/JHEP04(2014)169, arXiv:1402.7029.

[18] ATLAS Collaboration, "Search for direct production of charginos, neutralinos and sleptons in final states with two leptons and missing transverse momentum in pp collisions at $\sqrt{s} = 8$ TeV with the ATLAS detector", *JHEP* **05** (2014) 071, doi:10.1007/JHEP05(2014)071, arXiv:1403.5294.

[19] S. P. Martin, "A Supersymmetry primer", arXiv:hep-ph/9709356.

[20] J. Alwall, P. Schuster, and N. Toro, "Simplified Models for a First Characterization of New Physics at the LHC", *Phys.Rev.* **D79** (2009) 075020, doi:10.1103/PhysRevD.79.075020, arXiv:0810.3921.

[21] D.Alves et al., "Simplified Models for LHC New Physics Searches.", arXiv:1105.2838.

[22] ATLAS Collaboration, "Search for the direct production of charginos, neutralinos and staus in final states with at least two hadronically decaying taus and missing transverse momentum in pp collisions at $\sqrt{s}$ = 8 TeV with the ATLAS detector", *JHEP* **1410** (2014) 96, doi:10.1007/JHEP10(2014)096, arXiv:1407.0350.

[23] C. Lester and D. Summers, "Measuring masses of semiinvisibly decaying particles pair produced at hadron colliders", *Phys.Lett.* **B463** (1999) 99, doi:10.1016/S0370-2693(99)00945-4, arXiv:hep-ph/9906349.

[24] A. Barr, C. Lester, and P. Stephens, "m(T2): The Truth behind the glamour", *J.Phys.* **G29** (2003) 2343, doi:10.1088/0954-3899/29/10/304, arXiv:hep-ph/0304226.

[25] CMS Collaboration, "The CMS experiment at the CERN LHC", *JINST* **3** (2008) S08004, doi:10.1088/1748-0221/3/08/S08004.

[26] CMS Collaboration, "Particle–Flow Event Reconstruction in CMS and Performance for Jets, Taus, and $E_{\mathrm{T}}^{\mathrm{miss}}$", CMS Physics Analysis Summary CMS-PAS-PFT-09-001, CERN, 2009.

[27] CMS Collaboration, "Commissioning of the Particle-flow Event Reconstruction with the first LHC collisions recorded in the CMS detector", CMS Physics Analysis Summary CMS-PAS-PFT-10-001, CERN, 2010.

[28] M. Cacciari, G. P. Salam, and G. Soyez, "The anti-k_t jet clustering algorithm", *JHEP* **04** (2008) 063, doi:10.1088/1126-6708/2008/04/063, arXiv:0802.1189.

[29] CMS Collaboration, "Determination of Jet Energy Calibration and Transverse Momentum Resolution in CMS", *JINST* **6** (2011) P11002, doi:10.1088/1748-0221/6/11/P11002, arXiv:1107.4277.

[30] M. Cacciari and G. P. Salam, "Pileup subtraction using jet areas", *Phys. Lett.* **B659** (2008) 119, doi:10.1016/j.physletb.2007.09.077, arXiv:0707.1378.

[31] CMS Collaboration, "Identification of b-quark jets with the CMS experiment", *JINST* **8** (2013) P04013, doi:10.1088/1748-0221/8/04/P04013, arXiv:1211.4462.

[32] CMS Collaboration, "Reconstruction and identification of τ lepton decays to hadrons and ν_τ at CMS", arXiv:1510.07488.

[33] J. Alwall et al., "MadGraph 5: going beyond", *JHEP* **06** (2011) 128, doi:10.1007/JHEP06(2011)128, arXiv:1106.0522.

[34] P. Nason, "A New method for combining NLO QCD with shower Monte Carlo algorithms", *JHEP* **11** (2004) 040, doi:10.1088/1126-6708/2004/11/040, arXiv:hep-ph/0409146.

[35] S. Frixione, P. Nason, and C. Oleari, "Matching NLO QCD computations with Parton Shower simulations: the POWHEG method", *JHEP* **11** (2007) 070, doi:10.1088/1126-6708/2007/11/070, arXiv:0709.2092.

[36] S. Alioli, P. Nason, C. Oleari, and E. Re, "NLO single-top production matched with shower in POWHEG: s- and t-channel contributions", *JHEP* **09** (2009) 111, doi:10.1088/1126-6708/2009/09/111, arXiv:0907.4076. [Erratum: doi:10.1007/JHEP02(2010)011].

[37] S. Alioli, P. Nason, C. Oleari, and E. Re, "A general framework for implementing NLO calculations in shower Monte Carlo programs: the POWHEG BOX", *JHEP* **06** (2010) 043, doi:10.1007/JHEP06(2010)043, arXiv:1002.2581.

[38] T. Sjöstrand, S. Mrenna, and P. Skands, "PYTHIA 6.4 physics and manual", *JHEP* **05** (2006) 026, doi:10.1088/1126-6708/2006/05/026, arXiv:hep-ph/0603175.

[39] N. Davidson et al., "Universal interface of TAUOLA: Technical and physics documentation", *Comput. Phys. Commun.* **183** (2012) 821, doi:10.1016/j.cpc.2011.12.009, arXiv:1002.0543.

[40] GEANT4 Collaboration, "GEANT4—a simulation toolkit", *Nucl. Instrum. Meth. A* **506** (2003) 250, doi:10.1016/S0168-9002(03)01368-8.

[41] CMS Collaboration, "The fast simulation of the CMS detector at LHC", *J.Phys.Conf.Ser.* **331** (2011) 032049, doi:10.1088/1742-6596/331/3/032049.

[42] K. Melnikov and F. Petriello, "Electroweak gauge boson production at hadron colliders through O(alpha(s)**2)", *Phys. Rev.* **D74** (2006) 114017, doi:10.1103/PhysRevD.74.114017, arXiv:hep-ph/0609070.

[43] R. Gavin, Y. Li, F. Petriello, and S. Quackenbush, "W Physics at the LHC with FEWZ 2.1", *Comput. Phys. Commun.* **184** (2013) 208, doi:10.1016/j.cpc.2012.09.005, arXiv:1201.5896.

[44] M. Czakon and A. Mitov, "Top++: A Program for the Calculation of the Top-Pair Cross-Section at Hadron Colliders", *Comput. Phys. Commun.* **185** (2014) 2930, doi:10.1016/j.cpc.2014.06.021, arXiv:1112.5675.

[45] J. M. Campbell, R. K. Ellis, and C. Williams, "Vector boson pair production at the LHC", *JHEP* **07** (2011) 018, doi:10.1007/JHEP07(2011)018.

[46] B. Fuks, M. Klasen, D. R. Lamprea, and M. Rothering, "Gaugino production in proton-proton collisions at a center-of-mass energy of 8 TeV", *JHEP* **10** (2012) 081, doi:10.1007/JHEP10(2012)081, arXiv:1207.2159.

[47] B. Fuks, M. Klasen, D. R. Lamprea, and M. Rothering, "Precision predictions for electroweak superpartner production at hadron colliders with RESUMMINO", *Eur. Phys. J. C* **73** (2013) 2480, doi:10.1140/epjc/s10052-013-2480-0, arXiv:1304.0790.

[48] B. Fuks, M. Klasen, D. R. Lamprea, and M. Rothering, "Revisiting slepton pair production at the Large Hadron Collider", *JHEP* **01** (2014) 168, doi:10.1007/JHEP01(2014)168, arXiv:1310.2621.

[49] A. J. Barr and C. Gwenlan, "The Race for supersymmetry: Using m(T2) for discovery", *Phys.Rev.* **D80** (2009) 074007, doi:10.1103/PhysRevD.80.074007, arXiv:0907.2713.

[50] UA1 Collaboration, "Experimental Observation of Isolated Large Transverse Energy Electrons with Associated Missing Energy at s**(1/2) = 540-GeV", *Phys.Lett.* **B122** (1983) 103, doi:10.1016/0370-2693(83)91177-2.

[51] UA2 Collaboration, "Observation of Single Isolated Electrons of High Transverse Momentum in Events with Missing Transverse Energy at the CERN anti-p p Collider", *Phys.Lett.* **B122** (1983) 476, doi:10.1016/0370-2693(83)91605-2.

[52] CDF Collaboration, "Measurement of the *W* boson mass with the Collider Detector at Fermilab", *Phys.Rev.* **D64** (2001) 052001, doi:10.1103/PhysRevD.64.052001, arXiv:hep-ex/0007044.

[53] D0 Collaboration, "Improved *W* boson mass measurement with the DØ detector", *Phys.Rev.* **D66** (2002) 012001, doi:10.1103/PhysRevD.66.012001, arXiv:hep-ex/0204014.

[54] CMS Collaboration, "Performance of Electron Reconstruction and Selection with the CMS Detector in Proton-Proton Collisions at $\sqrt{s} = 8$ TeV", *JINST* **10** (2015) P06005, doi:10.1088/1748-0221/10/06/P06005, arXiv:1502.02701.

[55] CMS Collaboration Collaboration, "Performance of CMS muon reconstruction in pp collision events at $\sqrt{s} = 7$ TeV", *JINST* **7** (2012) P10002, doi:10.1088/1748-0221/7/10/P10002, arXiv:1206.4071.

[56] CMS Collaboration, "Measurement of the inclusive Z cross section via decays to tau pairs in pp collisions at $\sqrt{s} = 7$ TeV", *JHEP* **08** (2011) 117, doi:10.1007/JHEP08(2011)117, arXiv:1104.1617.

[57] CMS Collaboration, "Search for neutral MSSM Higgs bosons decaying to a pair of tau leptons in pp collisions", *JHEP* **1410** (2014) 160, doi:10.1007/JHEP10(2014)160, arXiv:1408.3316.

[58] G. Antchev et al., "First measurement of the total proton-proton cross section at the LHC energy of $\sqrt{s}$ =7 TeV", *Europhys. Lett.* **96** (2011) 21002, doi:10.1209/0295-5075/96/21002, arXiv:1110.1395.

[59] CMS Collaboration, "CMS Luminosity Based on Pixel Cluster Counting - Summer 2013 Update", CMS Physics Analysis Summary CMS-PAS-LUM-13-001, CERN, 2013.

[60] A. L. Read., "Presentation of search results: the CLs technique.", *J.Phys.G: Nucl. Part. Phys.* **28** (2002).

[61] LEP SUSY Working Group (ALEPH, DELPHI, L3, OPAL). Notes LEPSUSYWG/04-01.1.